An Adaptive Optimization-Based Load Shedding Scheme in Microgrids

Amin Gholami, Tohid Shekari, and Xu Andy Sun
Georgia Institute of Technology, Atlanta, Georgia 30332, USA
Email: a.gholami@gatech.edu, t.shekari@gatech.edu, andy.sun@isye.gatech.edu

Abstract

This paper proposes an adaptive optimization-based approach for under frequency load shedding (UFLS) in microgrids (μGs) following an unintentional islanding. In the first step, the total amount of load curtailments is determined based on the system frequency response (SFR) model. Then, the proposed mixed-integer linear programming (MILP) model is executed to find the best location of load drops. The novel approach specifies the least cost load shedding scenario while satisfying network operational limitations. A look-up table is arranged according to the specified load shedding scenario to be implemented in the network if the islanding event occurs in the μG. To be adapted with system real-time conditions, the look-up table is updated periodically. The efficiency of the proposed framework is thoroughly evaluated in a test μG with a set of illustrative case studies.

Nomenclature

Indices, Sets, and Mappings

b	Load block index.
g	Distributed generation (DG) index.
i, j	Bus indices.
p	Cosine linearization segment index.
r	Renewable energy source (RES) index.
Ω_{B_i}	Set of load blocks at bus i.
Ω_L	Set of lines.
Ω_G/Ω_{RES}	Set of DGs/RESs.
Ω_N	Set of microgrid (μG) buses.
Ω_P	Set of cosine linearization segments.
$\mathcal{M}_G/\mathcal{M}_{RES}$	Mapping of the set of DGs/RESs into the set of buses.

Parameters

B^B	Break point in cosine linearization segments.
C^B	Cosine value in the associated break point.
$H/D/R$	DG inertia/damping coefficient/governor droop.
G/B	Conductance/susceptance of line.
M, M'	Sufficiently large positive numbers.
$\overline{p}^D/\overline{q}^D$	Pre-fault active/reactive power consumption of load obtained from state estimation (SE).
p^{RES}/q^{RES}	Pre-fault active/reactive power production of RES obtained from SE.
$p^{G,0}$	Active power generation of DG before the load shedding.
P^M	μG pre-fault energy exchange with the upstream grid obtained from SE.
P^M_{thr}	The minimum amount of P^M which activates the load shedding process.
$P^M_{thr,SSF/DF}$	Steady-state/dynamic threshold of P^M.
p^{Shed}	Minimum total amount of load drops.
$p^{Shed}_{SSF}/p^{Shed}_{DF}$	Total amount of load shedding satisfying steady-state/dynamic frequency limitation.
R^U/R^D	Ramp-up/down limit of DG.
S	Capacity (apparent power) of DG.
t^{Shed}/t^{min}	Instants when the load shedding is implemented and minimum dynamic frequency occurs.
V^*	Pre-fault bus voltage magnitude obtained from SE.
τ^T/τ^V	Turbine/governor valve time constant of DG.
λ^{VOLL}	Value of lost loads (VOLL).
$\kappa^{PI}/\kappa^{PC}/\kappa^{PP}$	Coefficient of constant impedance/constant current/constant power term in active power load.
$\kappa^{QI}/\kappa^{QC}/\kappa^{QP}$	Coefficient of constant impedance/constant current/constant power term in reactive power load.
$\Delta f_{SSF}/\Delta f_{DF}$	Steady-state/nadir value of frequency deviation.
$\alpha_1, \alpha_2, \alpha_3, \beta_1, \beta_2, \beta_3, \varpi, m_1, m_2, m_3, c_1, c_2, c_3, \phi, \delta_1, \delta_2, \delta_3, \delta_4$	Axillary continuous parameters.

URI: http://hdl.handle.net/10125/50225
ISBN: 978-0-9981331-1-9

Variables

f^P/f^Q	Active/reactive power flow of line.
I	Current flow of line.
p^G/q^G	Active/reactive power output of DG following the load shedding process.
p^D/q^D	Active/reactive power consumption of load following the load shedding process.
V	Voltage magnitude of bus following the load shedding process.
x	Binary variable indicating the load shedding status of load (0/1).
α^P/α^Q	Axillary continuous variable.
ω	Piecewise linear approximation of $cos\,(\theta_i - \theta_j)$.
s/v	Positive/binary variable used in cosine linearization.

Symbols and Functions

$u\,(\bullet)$	Unit step function.
$(\bullet)^{\min\,/\,\max}$	Symbol for variable lower/upper limit.

1. Introduction

In recent years, the proliferation of distributed energy resources (DERs) has led to an increase in on-site electricity service procurement for customers. This new trend has a set of advantages and disadvantages over the conventional centralized power generation paradigm in terms of reliability, cost of maintenance, economies of scale, resiliency, and sustainability, to name a few [1]. Moreover, deploying DERs in a widespread and efficient manner requires practical mechanisms to identify and resolve the challenges of integration. In this context, microgrids (μGs) are emerging as a flexible way to aggregate DERs. The Department of Energy (DOE) defines a μG as "a group of interconnected loads and DERs within clearly defined electrical boundaries that acts as a single controllable entity with respect to the grid. A μG can connect and disconnect from the grid to enable it to operate in both grid-connected or island mode" [2].

An unintentional islanding usually occurs in μGs in the event of unforeseen faults in the upstream grid. IEEE 929-1988 Std. [3] necessitates the disconnection of DERs once the unintentional islanding event happens in the μG. Furthermore, IEEE 1547-2003 Std. [4] enforces DERs to detect the unintentional islanding and cease energizing the μG within maximum 2 sec. following the islanding event. Therefore, in the case of unintentional islanding, blackouts seem inevitable.

It goes without saying that the current practice of disconnecting the DERs following an islanding event is not economical since it imposes immense costs on the μG. When a μG with DERs is islanded, usually the frequency will change. The frequency will either go up if there is excess generation or down if there is excess load. The former can be controlled by reducing the output power of the distributed generators (DGs) or other DERs [5]. However, coping with the latter is more challenging. It is worth mentioning that in the normal operating condition, photovoltaic (PV) systems usually use maximum power point tracking and variable speed wind turbines optimize power coefficient (C_p) to produce maximum power. Thus, if all of the DGs are operating at maximum power and the frequency still goes down, some loads have to be shed to bring the frequency back to the allowable range. Nonetheless, it is possible that PV generators and wind turbines withhold production (these resources are non-dispatchable, but curtailable), and this is a growing trend in power system operation which provides further flexibility.

To address the weaknesses of conventional under frequency load shedding (UFLS) scheme, researchers have proposed adaptive load shedding schemes, which can be classified into two main categories: decentralized and centralized algorithms. Decentralized approaches use local voltage and frequency signals at each bus to make the decision about the load shedding process at that bus. Indeed, using these algorithms, the location, speed, and the amount of load curtailments are adjusted adaptively to preserve the system stability following severe incidents.

Centralized methods, on the other hand, use the data gathered from the grid in order to decide which load to be shed. The centralized schemes proposed in [6] drop loads at different buses based on their VQ margin and post-fault voltage magnitude. Reference [7] adopts both voltage and frequency information provided by phasor measurement units (PMUs) to implement the appropriate load shedding scenario in the network. Other centralized methods determine the amount and location of load drops according to the complete post-fault information about the network [8]–[11].

Owing to the differences between μGs and bulk power systems, the load shedding mechanism for a μG should be treated differently. μGs usually have small generators and, hence, small inertia. As a consequence, the frequency declines more rapidly in μGs. This paper presents a centralized adaptive optimization-based load shedding scheme to curtail the minimum amount of loads to preserve the μG stability following an unintentional islanding event. The developed technique arranges a look-up table including the optimum amount and location of load curtailments. The main contributions of the new methodology can be summarized as follows:

1) Given a specific amount of power exchange between the μG and the upstream grid, the optimal total

amount of load shedding is determined. Specifically, this value depends on the response of both the generators and the loads to the islanding event. These responses are reflected in the system frequency response (SFR) model as well as the μG dynamic and static frequency limitations.

2) We developed a mixed-integer linear programming (MILP) model for obtaining the amount of load drops at different buses. In the optimization model, an approximation of the μG AC operational limitations are considered to ensure the network security following the islanding event.
3) A hierarchical structure is proposed in this paper so as to reduce both data and communication requirements of the new centralized algorithm. To give more explanation, the majority of the needed information are periodically updated and only a practically tractable share is gathered in real time.

The rest of this paper is organized as follows. Section 2 presents the overview of the proposed load shedding algorithm. In Section 3, a method for estimating the total amount of load curtailments is developed. Section 4 is devoted to introducing the optimization-based load shedding scheme. Section 5 exhibits the efficiency of the novel approach using an illustrative case study. Eventually, conclusion is given in Section 6.

2. Overview of the Proposed Load Shedding Algorithm

The general framework of the proposed load shedding algorithm is depicted in Fig. 1. In the first step, the μG master controller (μGMC) gathers the network data periodically (e.g., $\Delta T = 5$ min.) and runs the state estimation (SE) in order to obtain the proposed scheme's input parameters (operating point of the μG, load and generation data, and μG topology). Then, the optimum total amount of load curtailments is determined based on the μG SFR model and the power exchange between the μG and the upstream grid. Note that the obtained total amount of load drops satisfies the μG dynamic and static frequency limitations. The total amount of load shedding along with the SE data are fed into the proposed optimization model in order to arrange a look-up table including the location of load drops as well as appropriate post load shedding strategies. On the other side, the status of point of common coupling (PCC) circuit breaker is monitored using indication (i.e., binary) data. If an unintentional islanding happens and the amount of power mismatch is greater than a specific value, the pre-specified load shedding scenarios will be implemented in the μG. Detailed explanations about different parts of the proposed methodology are provided in the following sections.

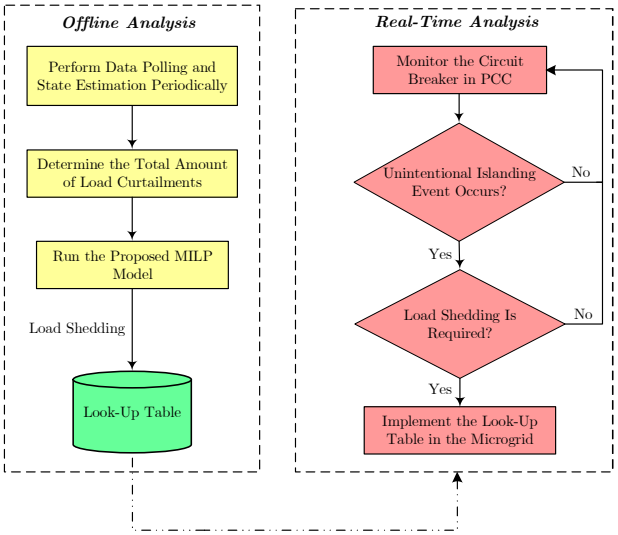

Figure 1. The general framework of the proposed load shedding algorithm.

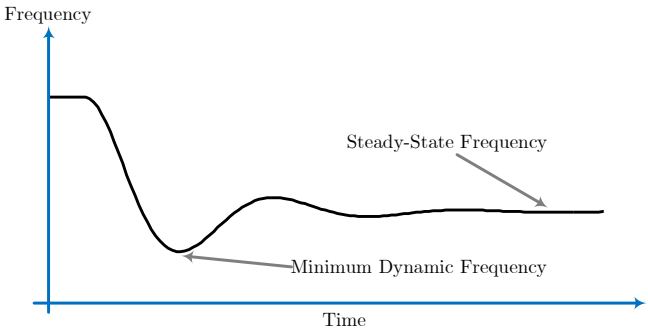

Figure 2. A typical frequency response of a μG following an unintentional islanding event.

3. Optimal Amount and Threshold for Activation of Load Shedding

The aim of this section is to determine the minimum amount of load curtailments as well as a threshold for activation of the load shedding process, while the μG dynamic and steady-state frequency limitations are satisfied. The minimum dynamic and steady-state frequencies are indicated in a typical frequency response of a μG following an unintentional islanding event, Fig. 2.

3.1. Frequency Response of the μG to an Islanding Event

As the first step, the frequency response of the μG to an islanding event should be specified. To do so, we use the aggregated SFR model of the μG as shown in Fig. 3 [12], [13]. This model is an equivalent single machine

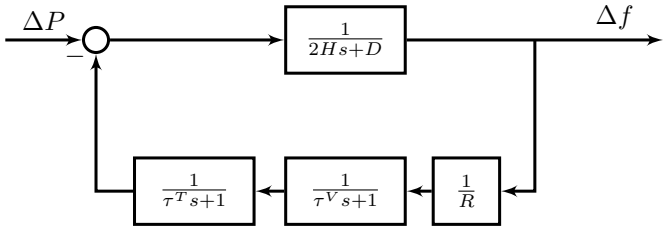

Figure 3. Block diagram of the adopted SFR model.

model of all DGs in the μG, where the frequency of the center of inertia is considered by ignoring intermachine oscillations. The transfer function $\frac{1}{2Hs+D}$ in the forward path represents the swing equation of the equivalent DG as well as the effects of the μG loads which are lumped into a single damping constant D. Moreover, the transfer functions in the feedback loop are associated with the governor droop, governor time constant, and turbine time constant of the equivalent DG [13].

The transfer function of the adopted SFR model can be written as (1).

$$\mathcal{H}(s) = \frac{\alpha_1 s^2 + \alpha_2 s + \alpha_3}{s^3 + \beta_1 s^2 + \beta_2 s + \beta_3}, \tag{1}$$

where

$$\alpha_1 = \frac{1}{2H}, \alpha_2 = \frac{1}{2H}\left(\frac{1}{\tau^T} + \frac{1}{\tau^V}\right), \alpha_3 = \frac{1}{2H\tau^T\tau^V}$$
$$\beta_1 = \frac{D}{2H} + \frac{1}{\tau^T} + \frac{1}{\tau^V}, \beta_2 = \frac{1}{\tau^T\tau^V} + \frac{D}{2H}\left(\frac{1}{\tau^T} + \frac{1}{\tau^V}\right)$$
$$\beta_3 = \frac{\frac{1}{R} + D}{2H\tau^T\tau^V}.$$

3.2. Threshold for Activation of Load Shedding Scheme

In the wake of an unintentional islanding, the governors and loads in the μG will respond to the incident, thereby compensating for a portion of power mismatch. Consequently, load shedding is not necessary in all cases. Specifically, the minimum amount of power mismatch which would activate the load shedding process is obtained by (2).

$$P^M_{thr} = \min\left\{P^M_{thr,SSF}, P^M_{thr,DF}\right\}, \tag{2}$$

where $P^M_{thr,SSF}$ and $P^M_{thr,DF}$ are the steady-state and dynamic thresholds of P^M, respectively. Suppose that the μG is not equipped with any load shedding scheme. In this condition, if an unintentional islanding happens, the input power deviation of the SFR model in Fig. 3 is defined as (3).

$$\Delta P(t) = -P^M u(t), \Delta P(s) = \frac{-P^M}{s}. \tag{3}$$

Hence, the Laplace form of the frequency deviation function is obtained as (4).

$$\Delta f(s) = \mathcal{H}(s)\Delta P(s) = \overbrace{\frac{\alpha_1 s^2 + \alpha_2 s + \alpha_3}{s\left(s^3 + \beta_1 s^2 + \beta_2 s + \beta_3\right)}}^{\mathcal{F}(s)}\left(-P^M\right). \tag{4}$$

Accordingly, $\mathcal{F}(s)$ can be decomposed into three terms using partial-fraction decomposition as follows:

$$\begin{aligned}\mathcal{F}(s) =& \frac{\alpha_1 s^2 + \alpha_2 s + \alpha_3}{s\left(s^3 + \beta_1 s^2 + \beta_2 s + \beta_3\right)} \\ =& \frac{\delta_1}{s} + \frac{\delta_2}{s - m_1} + \frac{\delta_3 s + \delta_4}{s^2 + m_2 s + m_3},\end{aligned} \tag{5}$$

where

$$m_2 = \frac{2}{3}\left(\beta_1 - \frac{c_1}{2} - \frac{c_2}{2c_1}\right),$$
$$m_3 = \frac{1}{9}\left[\left(\beta_1 - \frac{c_1}{2} - \frac{c_2}{2c_1}\right)^2 + \frac{3}{4}\left(c_1 - \frac{c_2}{c_1}\right)^2\right],$$
$$c_1 = \sqrt[3]{\frac{c_3 + \sqrt{c_3^2 - 4c_2^3}}{2}}, m_1 = \frac{-1}{3}\left(\beta_1 + c_1 + \frac{c_2}{c_1}\right),$$
$$c_2 = \beta_1^2 - 3\beta_2, c_3 = 2\beta_1^3 - 9\beta_1\beta_2 + 27\beta_3,$$
$$\delta_1 = \frac{\alpha_3}{\beta_3}, \delta_2 = \frac{\alpha_1 m_1^2 + \alpha_2 m_1 + \alpha_3}{m_1^3 + m_2 m_1^2 + m_3 m_1},$$
$$\delta_3 = -\left(\delta_1 + \delta_2\right), \delta_4 = \left(\delta_1\beta_2 + \delta_2 m_3 - \alpha_2\right)/m_1.$$

Taking the inverse Laplace transform of $\mathcal{F}(s)$, $\mathcal{F}(t)$ is given by:

$$\mathcal{F}(t) = \left(\delta_1 + \delta_2 e^{m_1 t} + \frac{\delta_3 e^{\frac{-m_2}{2}t}}{cos(\phi)} cos(\varpi t + \phi)\right) u(t), \tag{6}$$

where

$$\varpi = \sqrt{m_3 - \frac{m_2^2}{4}}, cos\phi = \frac{\varpi}{\sqrt{\varpi^2 + \left(\frac{m_2}{2} - \frac{\delta_3}{\delta_4}\right)^2}}.$$

Therefore, $\Delta f(t)$ can be written as (7).

$$\Delta f(t) = -P^M \mathcal{F}(t). \tag{7}$$

3.2.1. Steady-State Threshold of P^M. Given $\Delta f(t)$ as (7), Δf_{SSF} (i.e., steady state frequency deviation) can be computed as (8).

$$\Delta f_{SSF} = \lim_{t\to\infty} \Delta f(t) = \left(-P^M\right)\delta_1. \tag{8}$$

The load shedding process will be triggered if the value of Δf_{SSF} exceeds a given threshold $\Delta f^{\max}_{SSF}$, that is:

$$\left|\left(-P^M\right)\delta_1\right| \geq \left|\Delta f^{\max}_{SSF}\right|. \tag{9}$$

Therefore, the minimum amount of P^M which violates the steady-state frequency limitation, and thus, triggers the load shedding process is acquired as follows:

$$P^M \geq |\Delta f_{SSF}^{\max}| \left(D + \frac{1}{R} \right). \tag{10}$$

Accordingly, we define the right hand side of (10) as the steady state threshold of P^M.

3.2.2. Dynamic Threshold of P^M. The time when the frequency nadir happens (i.e., when the lowest frequency is reached before the frequency starts to recover) can be calculated by putting the first derivative of $\Delta f\left(t\right)$ equal to zero:

$$t_{\min} = \min \left\{ t : t > 0, \frac{d\Delta f\left(t\right)}{dt} = 0 \right\}. \tag{11}$$

Accordingly, the second trigger for the load shedding process is associated with the violation of nadir frequency limitation, that is:

$$|\Delta f\left(t_{\min}\right)| \geq |\Delta f_{DF}^{\max}|. \tag{12}$$

The solution to this inequality in terms of P^M, will provide another criterion or lower bound (denoted by $P_{thr,DF}^M$ in (2)) for the activation of the load shedding process.

3.3. Optimal Amount of Load Shedding

The minimum total amount of load curtailments satisfying both steady-state and dynamic frequency limitations is calculated as (13).

$$p^{Shed} = \max \left\{ p_{SSF}^{Shed}, p_{DF}^{Shed} \right\}, \tag{13}$$

where p_{SSF}^{Shed} and p_{DF}^{Shed} are obtained as follows. Suppose that the load shedding scheme is implemented in the μG with a delay of t^{Shed}, subsequent to the unintentional islanding event. Accordingly, the input power deviation of the SFR model will be defined as (14).

$$\Delta P\left(t\right) = -P^M u\left(t\right) + p^{Shed} u\left(t - t^{Shed}\right). \tag{14}$$

Taking the Laplace transform of $\Delta P\left(t\right)$ yields

$$\Delta P\left(s\right) = \frac{1}{s}\left(-P^M + p^{Shed} e^{-t^{Shed}s} \right). \tag{15}$$

Hence, the Laplace form of the frequency deviation function is obtained as (16).

$$\Delta f\left(s\right) = \mathcal{F}(s)\left(-P^M + p^{Shed} e^{-t^{Shed}s} \right), \tag{16}$$

where, $\mathcal{F}\left(s\right)$ is obtained from (5). Taking the inverse Laplace transform of (16), $\Delta f\left(t\right)$ can be written as (17) below

$$\Delta f\left(t\right) = -P^M \mathcal{F}\left(t\right) + p^{Shed} \mathcal{F}\left(t - t^{Shed}\right), \tag{17}$$

where $\mathcal{F}\left(t\right)$ is calculated in (6).

3.3.1. Load Shedding Value Based on the Steady-State Frequency Limitation. Given $\Delta f\left(t\right)$ as (17), Δf_{SSF} can be computed as (18) [8].

$$\Delta f_{SSF} = \lim_{t\to\infty} \Delta f\left(t\right) = \left(-P^M + p_{SSF}^{Shed} \right) \delta_1. \tag{18}$$

Therefore, the minimum total amount of load shedding satisfying the steady-state frequency limitation (i.e., $|\Delta f_{SSF}| \leq |\Delta f_{SSF}^{\max}|$) is acquired as follows:

$$p_{SSF}^{Shed} = P^M - |\Delta f_{SSF}^{\max}| \left(D + \frac{1}{R} \right). \tag{19}$$

3.3.2. Load Shedding Value Based on the Dynamic Frequency Limitation. Similar to Section 3.2.2, the time when the frequency nadir happens is acquired by solving (11), where $\Delta f\left(t\right)$ is calculated according to (17). By applying the nadir frequency limitation (i.e., $|\Delta f_{DF}| \leq |\Delta f_{DF}^{\max}|$), the minimum amount of load shedding satisfying dynamic frequency limitation (i.e., p_{DF}^{Shed}) is obtained. It should be noted that the proposed method in this paper is aimed at bringing the frequency to the permissible range (according to $\Delta f_{SSF}^{\max}$ and $\Delta f_{DF}^{\max}$) with the minimum amount of load shedding. Obviously, the frequency should finally bring back to 60 Hz, but this transition can happen with a short delay (2-3 minutes) with the advantage of shedding fewer loads. Subsequent to load shedding, DERs will try to bring the frequency back to 60 Hz. If this cannot happen (e.g., due to some limitations in the output of DERs), further loads will be curtailed. This idea is consistent with the load-frequency control mechanisms which are done in three different successive steps (i.e., primary control, secondary control, tertiary control).

4. Optimization-Based Load Shedding Scheme

4.1. Basic Model

In this section, the basic model of the μG load shedding scheme is presented. The objective function and problem constraints are outlined as follows:

$$\min \sum_{i\in\Omega_N} \sum_{b\in\Omega_{B_i}} \lambda_{ib}^{VOLL} \left(1 - x_{ib}\right) \overline{p}_{ib}^{D} \tag{20}$$

subject to

$$\sum_{g:(g,i)\in\mathcal{M}_G} p_g^G + \sum_{r:(r,i)\in\mathcal{M}_{RES}} p_r^{RES} - \sum_{b\in\Omega_{B_i}} x_{ib} p_{ib}^D = \sum_{(i,j)\in\Omega_L} f_{(i,j)}^P, \forall i \in \Omega_N \tag{21}$$

$$\sum_{g:(g,i)\in\mathcal{M}_G} q_g^G + \sum_{r:(r,i)\in\mathcal{M}_{RES}} q_r^{RES} - \sum_{b\in\Omega_{B_i}} x_{ib}q_{ib}^D = \sum_{(i,j)\in\Omega_L} f_{(i,j)}^Q, \forall i \in \Omega_N \tag{22}$$

$$f_{(i,j)}^P = G_{(i,j)}\Big(V_i^2 - V_iV_jcos\left(\theta_i-\theta_j\right)\Big) - B_{(i,j)}\Big(V_iV_jsin\left(\theta_i-\theta_j\right)\Big), \forall\left(i,j\right)\in\Omega_L \tag{23}$$

$$f_{(i,j)}^Q = -B_{(i,j)}\Big(V_i^2 - V_iV_jcos\left(\theta_i-\theta_j\right)\Big) - G_{(i,j)}\Big(V_iV_jsin\left(\theta_i-\theta_j\right)\Big), \forall\left(i,j\right)\in\Omega_L \tag{24}$$

$$-f_{(i,j)}^{P,\max} \le f_{(i,j)}^P \le f_{(i,j)}^{P,\max}, \forall\left(i,j\right)\in\Omega_L \tag{25}$$

$$-f_{(i,j)}^{Q,\max} \le f_{(i,j)}^Q \le f_{(i,j)}^{Q,\max}, \forall\left(i,j\right)\in\Omega_L \tag{26}$$

$$f_{(i,j)}^P + f_{(j,i)}^P = \frac{G_{(i,j)}}{G_{(i,j)}^2+B_{(i,j)}^2}\left|I_{(i,j)}\right|^2 \le f_{(i,j)}^{P,Loss,\max} = \frac{G_{(i,j)}}{G_{(i,j)}^2+B_{(i,j)}^2}\left|I_{(i,j)}^{\max}\right|^2, \forall\left(i,j\right)\in\Omega_L \tag{27}$$

$$V_i^{\min} \le V_i \le V_i^{\max}, \forall i \in \Omega_N \tag{28}$$

$$p_{ib}^D = \overline{p}_{ib}^D\Big(\kappa_{ib}^{PI}(V_i/V_i^*)^2 + \kappa_{ib}^{PC}\left(V_i/V_i^*\right) + \kappa_{ib}^{PP}\Big), \forall i\in\Omega_N, b\in\Omega_{B_i} \tag{29}$$

$$q_{ib}^D = \overline{q}_{ib}^D\Big(\kappa_{ib}^{QI}(V_i/V_i^*)^2 + \kappa_{ib}^{QC}\left(V_i/V_i^*\right) + \kappa_{ib}^{QP}\Big), \forall i\in\Omega_N, b\in\Omega_{B_i} \tag{30}$$

$$-R_g^D \le p_g^G - p_g^{G,0} \le R_g^U, \forall g\in\Omega_G \tag{31}$$

$$p_g^{G,\min} \le p_g^G \le p_g^{G,\max}, \forall g\in\Omega_G \tag{32}$$

$$q_g^{G,\min} \le q_g^G \le q_g^{G,\max}, \forall g\in\Omega_G \tag{33}$$

$$\sum_{i\in\Omega_N}\sum_{b\in\Omega_{B_i}}(1-x_{ib})p_{ib}^D \ge p^{Shed} \tag{34}$$

$$x_{ib}\in\{0,1\}, \forall i\in\Omega_N, b\in\Omega_{B_i}. \tag{35}$$

The objective function, (20), is the load shedding cost in the μG, which should be minimized. λ_{ib}^{VOLL} is a socioeconomic parameter and varies for different types of loads (e.g., industrial, commercial, agricultural, residential, and general loads). The group of equations (21)–(24) is related to the AC power flow equations. Line flow limits and bus voltage constraints are modeled through (25)–(27) and (28), respectively. Incorporation of a suitable load model for μG loads plays an important role in power system stability studies [9]. Therefore, the active and reactive power demands at different buses are modeled with voltage-dependent load model referred to as ZIP model, (29)–(30) [14]. Constraints (31)–(33) revolve around DG's ramp-up and ramp-down limits (31) and active and reactive power generation limits of DGs (32)–(33). The minimum total load shedding constraint is expressed as (34), and finally, the status of loads is characterized by a binary variable in (35).

4.2. Linearization of the Basic Model

The developed problem in Section 4.1 is a mixed-integer nonlinear programming (MINLP) model. In order to attain computational efficiency, the nonlinear equations ought to be linearized. The nonlinear terms $x_{ib}p_{ib}^D$ and $x_{ib}q_{ib}^D$ in (21)–(22) and (34) are the product of a binary and continuous variables. We can linearize these terms with the big-M method by introducing auxiliary semi-continuous variables (i.e., $\alpha_{ib}^P \triangleq x_{ib}p_{ib}^D$ and $\alpha_{ib}^Q \triangleq x_{ib}q_{ib}^D$) and the set of equations (36)–(39). In order to reduce the integrality gap in the linearized version of the aforementioned constraints, Big-Ms (i.e., M_{ib} and M'_{ib}) should be as small as possible, and it is usually challenging to determine correct values for them to use for each specific implementation. However, in this particular application, we can set $M_{ib} = \overline{p}_{ib}^D$ and $M'_{ib} = \overline{q}_{ib}^D$, $\forall i\in\Omega_N, b\in\Omega_{B_i}$. Note that these data (i.e., the upper bounds of active and reactive loads) are usually available in any system.

Moreover, considering reasonable assumptions given in Table 1 [15], AC power flow equations are replaced by their piecewise linear approximation form as (40)–(49). Finally, considering the permissible range for bus voltage magnitudes at different buses (i.e., $0.9 \le V_i, V_i^* \le 1.1$), (29)–(30) can be reasonably approximated by (50)–(51) [9]. With these changes, the proposed model is transformed into an MILP model.

$$-\left(1-x_{ib}\right)M_{ib} \le \alpha_{ib}^P - p_{ib}^D \le M_{ib}\left(1-x_{ib}\right), \forall i\in\Omega_N, b\in\Omega_{B_i} \tag{36}$$

$$-x_{ib}M_{ib} \le \alpha_{ib}^P \le M_{ib}x_{ib}, \forall i\in\Omega_N, b\in\Omega_{B_i} \tag{37}$$

Table 1. Constituent Terms in the Linearized Power Flow Equations [15]

Term	Approximation	Max. Abs. Error
V_i^2	$2V_i - 1$	0.0025
$V_iV_jcos(\theta_i - \theta_j)$	$V_i + V_j + cos(\theta_i - \theta_j) - 2$	0.0253
$V_iV_jsin(\theta_i - \theta_j)$	$sin(\theta_i - \theta_j)$	0.0659
$sin(\theta_i - \theta_j)$	$\theta_i - \theta_j$	0.0553

$$-(1-x_{ib})M'_{ib} \le \alpha^Q_{ib} - q^D_{ib} \le M'_{ib}(1-x_{ib}), \forall i \in \Omega_N, b \in \Omega_{B_i} \quad (38)$$

$$-x_{ib}M'_{ib} \le \alpha^Q_{ib} \le M'_{ib}x_{ib}, \forall i \in \Omega_N, b \in \Omega_{B_i} \quad (39)$$

$$f^P_{(i,j)} = G_{(i,j)}\left(V_i - V_j - \omega_{(i,j)} + 1\right) - B_{(i,j)}(\theta_i - \theta_j), \forall (i,j) \in \Omega_L \quad (40)$$

$$f^Q_{(i,j)} = -B_{(i,j)}\left(V_i - V_j - \omega_{(i,j)} + 1\right) - G_{(i,j)}(\theta_i - \theta_j), \forall (i,j) \in \Omega_L \quad (41)$$

$$\omega_{(i,j)} = \sum_{p \in \Omega_P} s_{(i,j)p} C^B_p, \forall (i,j) \in \Omega_L \quad (42)$$

$$\theta_i - \theta_j = \sum_{p \in \Omega_P} s_{(i,j)p} B^B_p, \forall (i,j) \in \Omega_L \quad (43)$$

$$\sum_{p \in \Omega_P} s_{(i,j)p} = 1, \forall (i,j) \in \Omega_L \quad (44)$$

$$\sum_{p \in \Omega_P} v_{(i,j)p} = 1, \forall (i,j) \in \Omega_L \quad (45)$$

$$s_{(i,j)p_1} \le v_{(i,j)p_1}, \forall (i,j) \in \Omega_L \quad (46)$$

$$s_{(i,j)p} \le v_{(i,j)p} - v_{(i,j)(p-1)}, \forall (i,j) \in \Omega_L, p \in \Omega_P, p \ne \{p_1, p_n\} \quad (47)$$

$$s_{(i,j)p_n} \le v_{(i,j)(p_{n-1})}, \forall (i,j) \in \Omega_L \quad (48)$$

$$v_{(i,j)p_n} = 0, \forall (i,j) \in \Omega_L \quad (49)$$

$$p^D_{ib} = \overline{p}^D_{ib}\Big(\kappa^{PI}_{ib}\left(1 + 2(V_i - V^*_i)\right) + \kappa^{PC}_{ib}(V_i/V^*_i) + \kappa^{PP}_{ib}\Big), \forall i \in \Omega_N, b \in \Omega_{B_i} \quad (50)$$

$$q^D_{ib} = \overline{q}^D_{ib}\Big(\kappa^{QI}_{ib}\left(1 + 2(V_i - V^*_i)\right) + \kappa^{QC}_{ib}(V_i/V^*_i) + \kappa^{QP}_{ib}\Big), \forall i \in \Omega_N, b \in \Omega_{B_i}. \quad (51)$$

Table 2. Technical Data of DG Units

Parameter	Unit			
	DG_1	DG_2	DG_3	DG_4
$p^{DG,\min}$ (MW)	1	1	1	1
$p^{DG,\max}$ (MW)	4	3.38	3.38	4.72
$q^{DG,\min}$ (MW)	−0.5	−0.5	−0.5	−0.5
$q^{DG,\max}$ (MW)	2	2	2	2
R^U (MW/min.)	2.4	2.4	2.4	2.4
R^D (MW/min.)	2.4	2.4	2.4	2.4

Table 3. μG Dynamic Data [5], [18]

Parameter	Value	Parameter	Value
H (sec.)	2	τ^V (sec.)	0.1
D	1	τ^T (sec.)	0.5
R	0.05	t^{Shed} (msec.)	100
$\Delta f^{\max}_{SSF}$ (Hz)	0.2	$\Delta f^{\max}_{DF}$ (Hz)	0.5

5. Case Study and Performance Evaluation

5.1. System Model and Parameters

In this section, the performance of the proposed scheme for the μG load shedding problem is thoroughly evaluated using a large-scale μG. All simulations were conducted on a PC with Intel Core™ i5 CPU @2.67 GHz and 4 GB RAM. The optimization model was implemented in the GAMS® IDE environment. The MILP and MINLP models were solved with IBM ILOG CPLEX® and BONMIN solvers, respectively. The modified IEEE 33-bus test system, which is a radial medium voltage (i.e., 12.66 kV) distribution system, is used as the test μG in this paper. The system topology and components are depicted in Fig. 4 and the feeders and loads' data are obtained from [16] and [17]. The test μG includes three DGs, whose technical data are given in Table 2. Meanwhile, three wind turbines as RESs with a total capacity of 3 MW are installed at buses 14, 16, and 31. To have a more realistic study, the load at each node of the μG is divided into three load blocks. Furthermore, five different load types (i.e., general, residential, agricultural, commercial, and industrial) with different VOLLs are taken into account, Fig. 5 [9]. Finally, the test system's dynamic data can be found in Table 3.

5.2. Simulated Cases and Discussion

In this section, three different contingencies are simulated in the test system, Table 4. To evaluate the performance of the proposed methodology, it is compared with the conventional UFLS scheme. The amount and setting of conventional UFLS relays have been designed according to [19]. The simulation results are summarized in the following figures and tables. According to Fig. 6, the

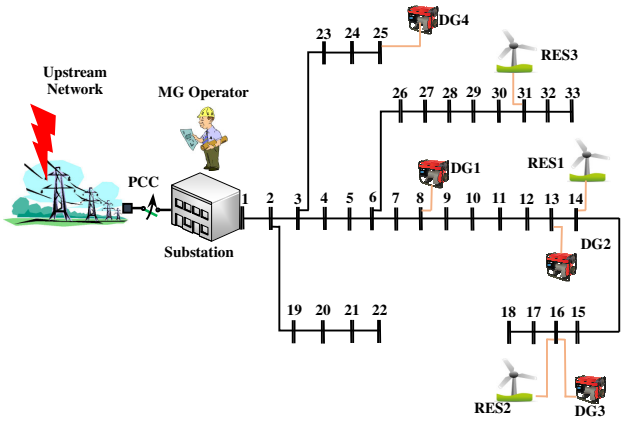

Figure 4. Single line diagram of the simulated μG [17].

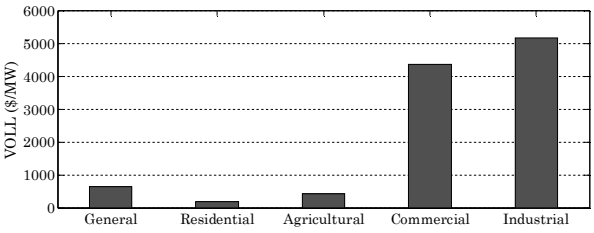

Figure 5. VOLL for different types of loads.

Table 4. Simulated Contingencies

Contingency No.	P^M (MW)	p^{Shed}_{SSF}	p^{Shed}_{DF}
1	3	1.81	1.7
2	4	2.81	2.86
3	5	3.81	4.15

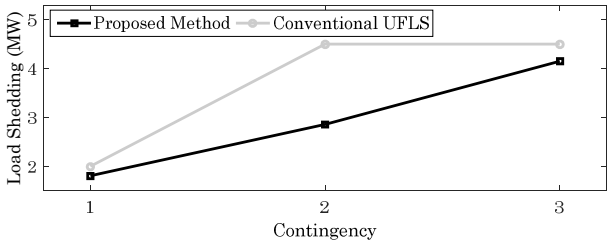

Figure 6. Comparison between the proposed and conventional UFLS methods in terms of load shedding.

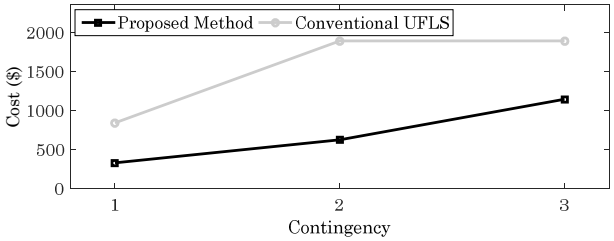

Figure 7. Comparison between the proposed and conventional UFLS methods in terms of load shedding cost.

amount of load shedding in the proposed method is less than that of the conventional UFLS approach. Considering the SFR model in the developed approach is the main reason of this observation. Similarly, the load shedding cost associated with the proposed method is much less than that of the conventional UFLS approach, Fig. 7. The reason is that in the conventional case, the locations of candidate loads to be shed are fixed, despite the fact that the VOLL of different feeders changes during the day. Therefore, in the conventional case, the interruption cost of dropped loads is not optimum around-the-clock. It is worth mentioning that in the proposed method, although the loads are shed according to their VOLL, operational limitations play a more important role. Indeed, the model is implemented in such a way that the load shedding cost is minimized, and at the same time, the network operational limitations are preserved.

As can be seen in Fig. 8, for all unintentional islanding events, minimum frequency of the μG is greater in the proposed approach due to its high speed in event indication and implementing the load shedding scenario. Taking a glance at Fig. 9 yields that the steady-state frequency of the μG following all contingencies is higher for the conventional UFLS method. On the other hand, the steady-state frequency associated with the proposed scheme is still in the safe range. Therefore, it can be inferred that the conventional method sheds non-optimal amount of loads encountering different events. These results prove that the proposed method is capable of preserving the system from collapsing and moving it to a new steady state and stable condition.

It is worth mentioning that keeping the bus voltages and line flows within the permissible range would guarantee a secure μG operation following the load shedding process. Therefore, if these constraints are violated in the network, the proposed methodology seeks to return them to the permissible range by modifying the available control variables.

Table 5 provides the curtailed load blocks in contingency 2 for both the nonlinear and linear optimization models, where differences are highlighted in red bold. In this contingency, the optimal values of the objective function for the nonlinear and linear models are \$623.4 and \$625.6, respectively. Accordingly, the load shedding costs are roughly equal in these two models, and the curtailed loads are identical in most cases. Moreover, Table 6 shows a comparison between the computation time of the two models, which has been obtained using a relative

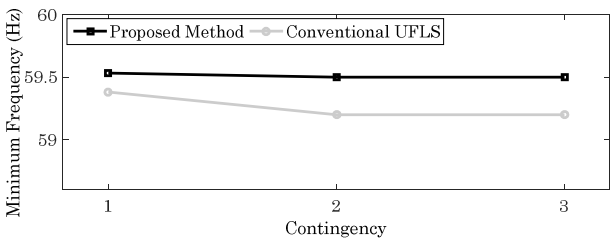

Figure 8. Comparison between the proposed and conventional UFLS methods in terms of minimum dynamic frequency.

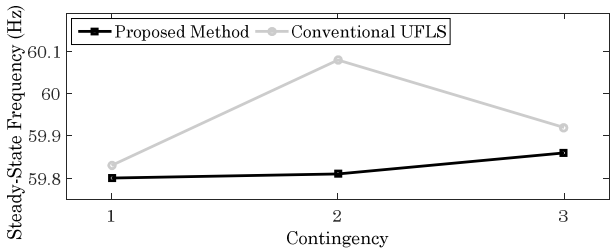

Figure 9. Comparison between the proposed and conventional UFLS methods in terms of steady-state frequency.

optimality criterion (i.e., Optcr) of 10^{-2}. As can be seen, the computation time is considerably diminished in the linear model, and this is highly effective in precarious situations such as the load shedding process, since prompt measures can keep electromechanical dynamics away from becoming stability threatening.

6. Conclusion

The proliferation of μGs all over the world has been remarkable in recent years, and their growth prospects in the future are astounding. μGs can improve the resilience of the grid based on their self-supply and island-mode capabilities. However, when a μG unintentionally enters the island mode, a considerable number of customers (or even all of them) are disconnected from the grid in order to maintain the load-generation equilibrium. New methodologies are therefore required to optimize the load shedding process in μGs. In this paper, an optimization-based load shedding model is presented as a promising tool to attain this goal. Mathematically, the load shedding model is formulated as a MILP problem. The structure of the proposed scheme reduces its communication requirements which is a major challenge in practice. The most relevant aspects of the proposed load shedding scheme are illustrated using a large-scale case study based on a 33-bus μG. It was observed that the proposed method sheds less amount of load in comparison with the conventional UFLS

Table 5. Comparison Between the Linear and Nonlinear Load Shedding Optimization Models

	Nonlinear Model			Linear Model		
	Load Block #			Load Block #		
Bus #	B1	B2	B3	B1	B2	B3
2	1.06			1.06		
3		0.96			0.96	
5		0.65			0.65	
6			**0.63**			
7						**2.22**
10		0.70	0.69		0.70	0.68
11					**0.51**	
12		0.67			0.67	
15		0.75	**0.71**		0.74	
16			0.68	**0.74**		0.67
17			0.69			0.68
18				**1.03**		
20	0.95		0.95	0.95		0.95
21			0.95			0.95
22	0.95			0.94		
24			4.62			4.61
25	4.72			4.72		
28		0.66			0.66	
30	2.16			2.16		
32			**2.42**			
33	0.67	**0.66**	0.70	0.67		0.69

Table 6. Computation Time of the Linear and Nonlinear Models

Contingency No.	Nonlinear model	Linear model
1	93 sec.	9 sec.
2	214 sec.	7 sec.
3	40 sec.	7 sec.

approach. Meanwhile, the developed structure outperformed the conventional scheme in terms of load shedding cost and minimum dynamic frequency following the load shedding process. Future studies could reformulate power flow equations for radial systems (since the complex power flow equations presented in this paper are not necessary for radial networks). Moreover, an unbalanced power flow model can be adopted to make the proposed load shedding method more practical in real world applications.

References

[1] J. A. Momoh, S. Meliopoulos, and R. Saint, "Centralized and distributed generated power systems-a comparison approach," *Future grid initiative white paper, PSERC*, pp. 1–33, 2012.

[2] D. T. Ton and M. A. Smith, "The U.S. Department of Energy's microgrid initiative," *The Electricity Journal*, vol. 25, no. 8, pp. 84–94, 2012.

[3] *Recommended Practice for Utility Interconnected Photovoltaic (PV) Systems*, IEEE Std. 929-2000, 2000.

[4] *IEEE Standard for Interconnecting Distributed Resources Into Electric Power Systems*, IEEE Std. 1547TM, Jun. 2003.

[5] P. Mahat, Z. Chen, and B. Bak-Jensen, "Under frequency load shedding for an islanded distribution system with distributed generators," *IEEE Trans. Power Del.*, vol. 25, no. 2, pp. 911–918, Apr. 2010.

[6] H. Seyedi and M. Sanaye-Pasand, "New centralized adaptive load shedding algorithms to mitigate power system blackouts," *IET Gener. Transm. Distrib.*, vol. 3, no. 1, pp. 99–114, Jan. 2009.

[7] J. Tang, J. Liu, F. Ponci, and A. Monti, "Adaptive load shedding based on combined frequency and voltage stability assessment using synchrophasor measurements," *IEEE Trans. Power Syst.*, vol. 28, no. 2, pp. 2035–2047, May 2013.

[8] T. Shekari, F. Aminifar, and M. Sanaye-Pasand, "An analytical adaptive load shedding scheme against severe combinational disturbances," *IEEE Trans. Power Syst.*, vol. 31, no. 5, pp. 4135–4143, Sept. 2016.

[9] T. Shekari, A. Gholami, F. Aminifar, and M. Sanaye-Pasand, "An adaptive wide-area load shedding scheme incorporating power system real-time limitations," *IEEE Syst. J.*, to be published.

[10] U. Rudez and R. Mihalic, "Wams-based under frequency load shedding with short-term frequency prediction," *IEEE Trans. Power Del.*, vol. 31, no. 4, pp. 1912–1920, Aug. 2016.

[11] V. V. Terzija, "Adaptive underfrequency load shedding based on the magnitude of the disturbance estimation," *IEEE Trans. Power Syst.*, vol. 21, no. 3, pp. 1260–1266, Aug. 2006.

[12] Y. Lu, W. Kao, and Y. Chen, "Study of applying load shedding scheme with dynamic d-factor values of various dynamic load models to taiwan power system," *IEEE Trans. Power Syst.*, vol. 20, no. 4, pp. 1976–1984, Nov. 2005.

[13] P. Kundur, *Power system stability and control*. McGraw–hill, New York, 1994.

[14] IEEE Task Force on Load Representation for Dynamic Performance, "Bibliography on load models for power flow and dynamic performance simulation," *IEEE Trans. Power Syst.*, vol. 10, no. 1, pp. 523–538, Feb. 1995.

[15] P. A. Trodden, W. A. Bukhsh, A. Grothey, and K. I. McKinnon, "Optimization-based islanding of power networks using piecewise linear ac power flow," *IEEE Trans. Power Syst.*, vol. 29, no. 3, pp. 1212–1220, May 2014.

[16] M. E. Baran and F. Wu, "Network reconfiguration in distribution system for loss reduction and load balancing," *IEEE Trans. Power Del.*, vol. 4, no. 2, pp. 1401–1407, Apr. 1989.

[17] A. Gholami, T. Shekari, F. Aminifar, and M. Shahidehpour, "Microgrid scheduling with uncertainty: the quest for resilience," *IEEE Trans. Smart Grid*, vol. 7, no. 6, pp. 2849–2858, Nov. 2016.

[18] A. Mokari-Bolhasan, H. Seyedi, B. Mohammadi-ivatloo, S. Abapour, and S. Ghasemzadeh, "Modified centralized ROCOF based load shedding scheme in an islanded distribution network," *Int. J. Elec. Power & Energy Syst.*, vol. 62, pp. 806–815, Nov. 2014.

[19] M. Abedini, M. Sanaye-Pasand, and S. Azizi, "Adaptive load shedding scheme to preserve the power system stability following large disturbances," *IET Gen. Transm. Distrib.*, vol. 8, no. 12, pp. 2124–2133, Dec. 2014.